ISSN 0915-633X

NATIONAL INSTITUTE FOR FUSION SCIENCE

Turbulence-driven Zonal Flows in Helical Systems with Radial Electric Fields

H. Sugama and T.-H. Watanabe

(Received - Dec. 3, 2008)

NIFS-948 Dec. 16, 2008

RESEARCH REPORT
NIFS Series

TOKI, JAPAN

This report was prepared as a preprint of work performed as a collaboration research of the National Institute for Fusion Science (NIFS) of Japan. The views presented here are solely those of the authors. This document is intended for information only and may be published in a journal after some rearrangement of its contents in the future.

Inquiries about copyright should be addressed to the Research Information Office, National Institute for Fusion Science, Oroshi-cho, Toki-shi, Gifu-ken 509-5292 Japan.

E-mail: bunken@nifs.ac.jp

<Notice about photocopying>

In order to photocopy any work from this publication, you or your organization must obtain permission from the following organizaion which has been delegated for copyright for clearance by the copyright owner of this publication.

Except in the USA

Japan Academic Association for Copyright Clearance (JAACC)
6-41 Akasaka 9-chome, Minato-ku, Tokyo 107-0052 Japan
Phone: 81-3-3475-5618 FAX: 81-3-3475-5619 E-mail: jaacc@mtd.biglobe.ne.jp

In the USA

Copyright Clearance Center, Inc.
222 Rosewood Drive, Danvers, MA 01923 USA
Phone: 1-978-750-8400 FAX: 1-978-646-8600

Turbulence-driven zonal flows in helical systems with radial electric fields

H. Sugama[1,2] and T.-H. Watanabe[1,2]
[1] *National Institute for Fusion Science, Toki 509-5292, Japan*
[2] *The Graduate University for Advanced Studies, Toki 509-5292, Japan*
(Dated: December 2, 2008)

Collisionless long-time responses of the zonal-flow potential to the initial condition and to the turbulence source in helical systems with radial electric fields are theoretically derived. All classes of particles in passing, toroidally-trapped, and helical-ripple-trapped states are considered and transitions between toroidally-trapped and helical-ripple-trapped states are taken into account to analytically solve the gyrokinetic equation by taking its average along the particle orbits. The zonal-flow responses are enhanced when the radial displacements of helical-ripple-trapped particles are reduced by neoclassical optimization of the helical geometry to lower the radial drift or by strengthening the radial electric field E_r to boost the poloidal rotation. Under the same conditions on the geometry and the magnitude of E_r, using ions with a heavier mass gives rise to a higher zonal-flow response, from which the turbulent transport is expected to show a more favorable ion-mass dependence than the conventional gyro-Bohm scaling.

Keywords: zonal flows, helical systems, gyrokinetics

PACS numbers:

I. INTRODUCTION

Zonal flows are now well known to play a critical role in regulation of turbulent transport in plasmas [1, 2]. From the viewpoint of improving plasma confinement, it is an important issue to investigate effects of magnetic configuration on zonal flows generated by turbulence. Theoretical works on collisionless time evolution of zonal flows in tokamaks [3–6] and in helical systems [7–12] such as heliotrons and stellarators elucidated how the zonal-flow response to a given turbulence source depends on the toroidal magnetic geometry by which particle orbits are determined. It was predicted in our previous works [7, 8] that the zonal-flow response can be increased in helical systems by reducing radial drift velocities of helical-ripple-trapped particles. This implies that helical configurations optimized for reducing neoclassical ripple transport [13–15] can simultaneously reduce the turbulent transport with enhancing zonal-flow generation. In fact, the theoretical prediction was confirmed by the ion temperature gradient (ITG) turbulence simulation using the gyrokinetic Vlasov (GKV) code [16–19] and it is consistent with the confinement improvement observed experimentally in the inward-shifted plasma in the Large Helical Device (LHD) [20, 21]. The reduction of anomalous transport by neoclassical optimization provides an attractive scenario for advanced concepts of helical devices [22–26].

In helical systems, the radial electric field E_r is produced from ambipolar particle fluxes [14] and it gives rise to the macroscopic $\mathbf{E}\times\mathbf{B}$ rotation, which is distinguished from the microscopic sheared $\mathbf{E}\times\mathbf{B}$ zonal flows. The $\mathbf{E}\times\mathbf{B}$ rotation driven by E_r, which was not taken into account in our original theory [7, 8], is expected to reduce not only neoclassical ripple transport but also turbulent transport through improving the zonal-flow response [10, 18, 19]. In the zonal-flow theory by Mynick and Boozer [10], the action-angle formalism is used to treat poloidally-closed $\mathbf{E}\times\mathbf{B}$-drift orbits of helical-ripple-trapped particles as well as bounce orbits of toroidally-trapped particles. However, for practical cases, such as in the LHD configuration, some helical-ripple-trapped particles cannot draw poloidally-closed orbits and transitions between toroidally-trapped and helical-ripple-trapped states can occur with some probability [14, 27]. Effects of these transitions are newly included in the preset work to present a more complete theory of zonal flows in helical system. This paper presents new formulas, from which we find how the helical geometry and E_r affect collisionless time evolution of zonal flows. The E_r effects appear through the poloidal Mach number defined by $M_p \equiv |(cE_r/B_0r_0)(R_0q/v_{ti})|$ with the safety factor q, the magnetic field strength B_0, the speed of light c, the minor (major) radius r_0 (R_0), and the ion thermal velocity $v_{ti} \equiv (T_i/m_i)^{1/2}$. Thus, when the geometry and the magnitude of E_r are fixed, a higher zonal-flow response is obtained by using ions with a heavier mass, which increases M_p, and the resultant turbulent transport is expected to show a more favorable ion-mass dependence than the conventional gyro-Bohm scaling [28].

Basic equations for describing zonal flows in helical systems are shown in Sec. II and analytical solutions of the distribution function are given in Sec. III, where we consider all classes of particle orbits and treat transitions between toroidally-trapped and helical-ripple-trapped particles in the presence of the radial electric field E_r. In Sec. IV, the collisionless long-time zonal-flow responses to the initial condition and to the ITG turbulence are derived with including effects of the helical geometry and E_r. Finally, conclusions are given in Sec. VI.

II. BASIC EQUATIONS

In the present work, we consider the same helical magnetic configuration as in Ref. [8]. We use the toroidal coordinates (r, θ, ζ), where r, θ, and ζ denote the flux surface label, the poloidal angle, and the toroidal angle, respectively. The magnetic field is written as $\mathbf{B} = \nabla\psi(r) \times \nabla(\theta - \zeta/q(r))$, where $2\pi\psi(r)$ is equal to the toroidal flux within the flux surface labeled r and $q(r)$ represents the safety factor. The magnetic field strength is written by a function of poloidal and toroidal angles (its r-dependence is not shown here for simplicity) as [8, 13]

$$B = B_0[1 - \epsilon_T(\theta) - \epsilon_H(\theta)\cos\{L\theta - M\zeta + \chi_H(\theta)\}], \tag{1}$$

where M (L) is the toroidal (main poloidal) period number of the helical field. For the LHD, $L = 2$ and $M = 10$. Here, it is assumed that $L/(qM) \sim \epsilon_T \sim \epsilon_H \ll 1$. In the present study, we put $\epsilon_T(\theta) = \epsilon_t \cos\theta$. Multiple-helicity effects from Fourier components $\propto \cos\{(L + n)\theta - M\zeta\}$ with $n = \pm 1, \pm 2, \cdots$ can be included in the function $\epsilon_H(\theta)$ [8, 13] which is even in θ and never take negative values. An example of the profile of the field strength along the field line $\zeta = q\theta$ is shown in Fig. 1.

The gyrokinetic equation [29] for the zonal flow component with the perpendicular wave number vector $\mathbf{k}_\perp = k_r\nabla r$ is given by

$$\left(\frac{\partial}{\partial t} + v_\parallel \mathbf{b}\cdot\nabla + i\omega_D + V_E\right) g_{\mathbf{k}_\perp} = \frac{e}{T}F_0 J_0(k_\perp\rho)\frac{\partial\phi_{\mathbf{k}_\perp}}{\partial t} + S_{\mathbf{k}_\perp}F_0, \tag{2}$$

where F_0 is the local equilibrium distribution function that takes the Maxwellian form, $J_0(k_\perp\rho)$ is the zeroth-order Bessel function, $\rho = v_\perp/\Omega$ is the gyroradius, and $\Omega = eB/(mc)$ is the gyrofrequency. Here, subscripts to represent particle species are dropped for simplicity. The drift frequency ω_D is defined by $\omega_D \equiv \mathbf{k}_\perp \cdot \mathbf{v}_d \equiv k_r v_{dr}$, where $v_{dr} = \mathbf{v}_d \cdot \nabla r$ is the radial component of the gyrocenter drift velocity and the radial coordinate r is defined by $\psi = B_0 r^2/2$. The $\mathbf{E} \times \mathbf{B}$ drift velocity $\mathbf{v}_E \equiv (c/B)E_r\nabla r \times \mathbf{b}$ due to the equilibrium radial electric field E_r is included in the differential operator $V_E \equiv \mathbf{v}_E \cdot \nabla$. In the present work, E_r is assumed to be constant. The source term $S_{\mathbf{k}_\perp}F_0$ on the right-hand side of Eq. (2) represents the $\mathbf{E} \times \mathbf{B}$ nonlinearity and is written as $S_{\mathbf{k}_\perp}F_0 = (c/B)\sum_{\mathbf{k}'_\perp + \mathbf{k}''_\perp = \mathbf{k}_\perp}[\mathbf{b} \cdot (\mathbf{k}'_\perp \times \mathbf{k}''_\perp)]J_0(k'_\perp\rho)\phi_{\mathbf{k}'_\perp} g_{\mathbf{k}''_\perp}$. In Eq. (2), $g_{\mathbf{k}_\perp}$ is regarded as a function of independent variables $(r, \theta, \zeta, \varepsilon, \mu)$, where $\varepsilon \equiv \frac{1}{2}mv^2 + e\Phi$ and $\mu \equiv mv_\perp^2/(2B)$ represent the particle's energy and magnetic moment, respectively. The gyrokinetic equation given in Eq. (2) is based on the ballooning representation [30] to describe the local structure of perturbations with much smaller perpendicular wave lengths than equilibrium scale lengths. We consider the local region around the magnetic surface $r = r_0$ and write the equilibrium electrostatic potential as $\Phi = -E_r x$, where $x \equiv r - r_0$.

As discussed in Ref. [18], although the potential fluctuation $\phi_{\mathbf{k}_\perp}$, which produces zonal flows, is constant on the flux surface, the solution $g_{\mathbf{k}_\perp}$ of Eq. (2) needs to have a dependence on the field line label $\alpha \equiv \zeta - q(r)\theta$ in helical systems because ω_D depends on α. Then, $V_E g_{\mathbf{k}_\perp}$ in Eq. (2) does not vanish and it yields effects of the equilibrium radial electric field on $g_{\mathbf{k}_\perp}$ and accordingly on behaviors of the zonal-flow potential. It is assumed in Eq. (2) that, compared to the magnitude of $\mathbf{v}_E$, components of grad B and curvature drift velocities parallel to $\nabla r \times \mathbf{b}$ are negligibly small.

The perturbed *particle* distribution function $\delta f_{\mathbf{k}_\perp}$ is written in terms of the electrostatic potential $\phi_{\mathbf{k}_\perp}$ and the solution $g_{\mathbf{k}_\perp}$ of Eq. (2) as

$$\delta f_{\mathbf{k}_\perp} = -\frac{e\phi_{\mathbf{k}_\perp}}{T}F_0 + g_{\mathbf{k}_\perp} e^{-i\mathbf{k}_\perp\cdot\boldsymbol{\rho}}, \tag{3}$$

where $\boldsymbol{\rho} = \mathbf{b} \times \mathbf{v}/\Omega$. The perturbed *gyrocenter* distribution function $\delta f^{(\mathrm{g})}_{\mathbf{k}_\perp}$ is given by

$$\delta f^{(\mathrm{g})}_{\mathbf{k}_\perp} = -J_0(k_\perp\rho)\frac{e\phi_{\mathbf{k}_\perp}}{T}F_0 + g_{\mathbf{k}_\perp}. \tag{4}$$

The perturbed gyrocenter distribution function $\delta f^{(\mathrm{g})}_{\mathbf{k}_\perp}$ and the nonadiabatic part $g_{\mathbf{k}_\perp}$ are independent of the gyrophase although the perturbed particle distribution function $\delta f_{\mathbf{k}_\perp}$ depends on it as seen from the factor $e^{-i\mathbf{k}_\perp\cdot\boldsymbol{\rho}}$ on the right-hand side of Eq. (3). Using Eqs. (3) and (4), we obtain

$$\delta f_{\mathbf{k}_\perp} = \delta f^{(\mathrm{g})}_{\mathbf{k}_\perp} e^{-i\mathbf{k}_\perp\cdot\boldsymbol{\rho}} - \frac{e\phi_{\mathbf{k}_\perp}}{T}F_0\left[1 - J_0(k_\perp\rho)e^{-i\mathbf{k}_\perp\cdot\boldsymbol{\rho}}\right]. \tag{5}$$

On the right-hand side of Eq. (5), the factor $e^{-i\mathbf{k}_\perp\cdot\boldsymbol{\rho}}$ in the first term results from the difference between the particle and gyrocenter positions while the second group of terms represent the classical polarization. The classical polarization refers to the variation of the particle distribution due to the potential perturbation in the magnetized plasma where particles are subject to gyromotion around field lines.

III. ANALYTICAL SOLUTION OF THE PERTURBED DISTRIBUTION FUNCTION

In this section, we analytically solve the gyrokinetic equation in Eq. (2) to obtain the perturbed distribution function, which determines the long-time behavior of zonal flows. For that purpose, different classes of collisionless particle orbits are investigated here.

Particles trapped in helical ripples are characterized by $\kappa^2 < 1$, where the trapping parameter κ defined by

$$\kappa^2 = \frac{\varepsilon - \mu B_0\{1 - \epsilon_T(\theta) - \epsilon_H(\theta)\} + eE_r x}{2\mu B_0\epsilon_H(\theta)}. \tag{6}$$

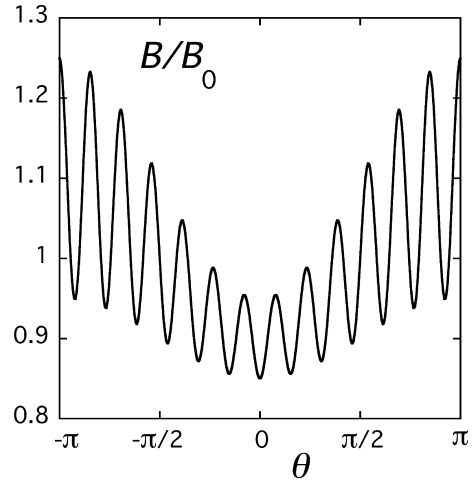

FIG. 1: An example of profile of the magnetic field strength along the field line ($\zeta = q\theta$). Here, $B/B_0 = 1 - \epsilon_t \cos\theta - \epsilon_H(\theta)\cos(L\theta - M\zeta)$, $L = 2$, $M = 10$, $q = 1.5$, $\epsilon_t = 0.1$, and $\epsilon_H(\theta) = 0.1 \times (1 - 0.5\cos\theta)$ are used.

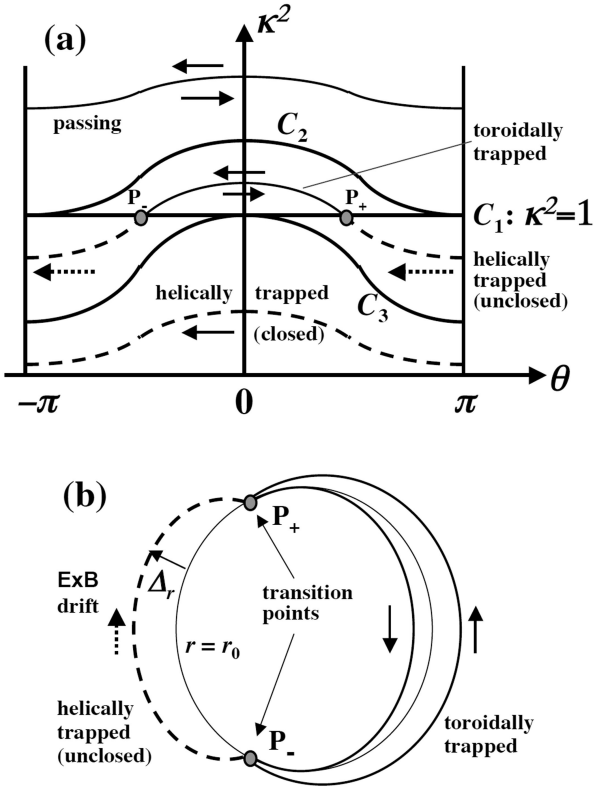

FIG. 2: Particle orbits in the (θ, κ^2)-plane (a) and poloidal cross sections of toroidally-trapped and helically-trapped orbits, between which transitions can occur (b). Dashed lines represent bounce-center $\mathbf{E} \times \mathbf{B}$-drift motions of helically-trapped particles. Transition points P_+ and P_- are located at poloidal angles $\theta = \theta_t$ and $-\theta_t$, respectively.

Using $L/(qM) \ll 1$, we approximate the field line element dl by $R_0 d\zeta$, where R_0 denotes the major radius of the toroid. Then, the orbital average within a helical ripple is defined by

$$\overline{A} = \begin{cases} \frac{1}{2}\sum_{\sigma=\pm1}\int_{\zeta_1}^{\zeta_2}(R_0 d\zeta/|v_\parallel|)A/\int_{\zeta_1}^{\zeta_2}(R_0 d\zeta/|v_\parallel|) \\ \qquad\qquad \text{for } \kappa^2 < 1 \\ \int_{\zeta_0-\pi/M}^{\zeta_0+\pi/M}(R_0 d\zeta/|v_\parallel|)A/\int_{\zeta_0-\pi/M}^{\zeta_0+\pi/M}(R_0 d\zeta/|v_\parallel|) \\ \qquad\qquad \text{for } \kappa^2 > 1, \end{cases} \tag{7}$$

where $\sigma = v_\parallel/|v_\parallel|$ is the sign of the parallel velocity, (ζ_1, ζ_2) represents the toroidal-angle interval for a particle trapped within a helical ripple, and $(\zeta_0 - \pi/M, \zeta_0 + \pi/M)$ corresponds to a whole helical ripple around the local minimum of B at $\zeta = \zeta_0$. Using the longitudinal adiabatic invariant J [13, 14, 27] given by

$$\begin{aligned} J &= \begin{cases} 2\int_{\zeta_1}^{\zeta_2} R_0 d\zeta\ |v_\parallel| & \text{for } \kappa^2 < 1 \\ \int_{\zeta_0-\pi/M}^{\zeta_0+\pi/M} d\zeta\ \left(R_0|v_\parallel| - \sigma\dfrac{e\psi' x}{mcq}\right) & \text{for } \kappa^2 > 1 \end{cases} \\ &= \begin{cases} 16\dfrac{R_0}{M}\left(\dfrac{\mu B_0\epsilon_H}{m}\right)^{1/2}[E(\kappa) - (1-\kappa^2)K(\kappa)] \\ \qquad\qquad \text{for } \kappa^2 < 1 \\ -\sigma\dfrac{2\pi}{M}\dfrac{e\psi' x}{mcq} + 8\dfrac{R_0}{M}\left(\dfrac{\mu B_0\epsilon_H}{m}\right)^{1/2}\kappa E(\kappa^{-1}) \\ \qquad\qquad \text{for } \kappa^2 > 1, \end{cases} \end{aligned} \tag{8}$$

and the time period τ_h given by

$$\begin{aligned} \tau_h &= m\frac{\partial J(\varepsilon,\theta,x,\mu)}{\partial\varepsilon} = \begin{cases} 2\int_{\zeta_1}^{\zeta_2} R_0 d\zeta/|v_\parallel| & \text{for } \kappa^2 < 1 \\ \int_{\zeta_0-\pi/M}^{\zeta_0+\pi/M} R_0 d\zeta/|v_\parallel| & \text{for } \kappa^2 > 1 \end{cases} \\ &= \begin{cases} 4(R_0/M)(\mu B_0\epsilon_H/m)^{-1/2}K(\kappa) \\ \qquad\qquad \text{for } \kappa^2 < 1 \\ 2(R_0/M)(\mu B_0\epsilon_H/m)^{-1/2}\kappa^{-1}K(\kappa^{-1}) \\ \qquad\qquad \text{for } \kappa^2 > 1, \end{cases} \end{aligned} \tag{9}$$

with the complete elliptic integrals $K(\kappa)$ and $E(\kappa)$, the orbital average of the radial drift velocity within a helical ripple is given by

$$\begin{aligned} \overline{v}_{dr} &= \frac{mc}{e\psi'\tau_h}\frac{\partial J(\varepsilon,\theta,x,\mu)}{\partial\theta} = -\frac{c}{e\psi'}\frac{\partial H(\theta,x,\mu,J)}{\partial\theta} \\ &= \begin{cases} \dfrac{c\mu B_0}{e\psi'}\left[\dfrac{\partial\epsilon_H}{\partial\theta}\left\{\dfrac{2E(\kappa)}{K(\kappa)} - 1\right\} + \dfrac{\partial\epsilon_T}{\partial\theta}\right] \\ \qquad\qquad \text{for } \kappa^2 < 1 \\ \dfrac{c\mu B_0}{e\psi'}\left[\dfrac{\partial\epsilon_H}{\partial\theta}\left\{2\kappa^2\left(\dfrac{E(\kappa^{-1})}{K(\kappa^{-1})} - 1\right) + 1\right\} + \dfrac{\partial\epsilon_T}{\partial\theta}\right] \\ \qquad\qquad \text{for } \kappa^2 > 1, \end{cases} \end{aligned} \tag{10}$$

where $\psi' = B_0 r_0$. Similarly, the averaged poloidal angu-

lar velocity ω_θ is written as

$$\omega_\theta = -\frac{mc}{e\psi'\tau_h}\frac{\partial J(\varepsilon,\theta,x,\mu)}{\partial x} = \frac{c}{e\psi'}\frac{\partial H(\theta,x,\mu,J)}{\partial x} = \begin{cases} -\dfrac{cE_r}{\psi'} & \text{for } \kappa^2 < 1 \\ \dfrac{2\pi\sigma}{qM\tau_h} - \dfrac{cE_r}{\psi'} & \text{for } \kappa^2 > 1, \end{cases} \tag{11}$$

where the functions $J(\varepsilon,\theta,x,\mu)$ and $\varepsilon = H(\theta,x,\mu,J)$ are defined from substituting Eq. (6) into Eq. (8). The x-dependence enters J and H through eE_rx in Eq. (6), where other x-dependences in $\mu B_0(1-\epsilon_T-\epsilon_H)$ and in $\mu B_0\epsilon_H$ are neglected. Thus, the $\mathbf{E}\times\mathbf{B}$ drift appears in Eq. (11) while the grad B and curvature drifts don't.

The parallel derivative is rewritten as $\mathbf{b}\cdot\nabla \simeq R_0^{-1}(\partial/\partial\zeta + q^{-1}\partial/\partial\theta)$. Then, we use $(\partial g_{\mathbf{k}_\perp}/\partial\theta)/(\partial g_{\mathbf{k}_\perp}/\partial\zeta) \sim r_0/R_0 \ll 1$ and $V_E g_{\mathbf{k}_\perp} \simeq -(cE_r/B_0r_0)(\partial g_{\mathbf{k}_\perp}/\partial\theta)$ in Eq. (2). Also, we replace $\omega_D(=k_rv_{dr})$ with $\overline{\omega}_D(=k_r\overline{v}_{dr})$, which is justified because the radial displacement δ_r [see Eq. (26) in Ref. [8]] of the gyrocenter from the helical-ripple-averaged radial position is much smaller than the gyroradius ρ for helical systems with $M \gg 1$. Based on these approximations, we obtain the lowest-order equation $(v_\parallel/R_0)(\partial g_{\mathbf{k}_\perp}/\partial\zeta) = 0$ from Eq. (2), where $\partial g_{\mathbf{k}_\perp}/\partial t$ is dropped because the long-time behavior of zonal flows with characteristic frequencies much smaller than $v_\parallel/(R_0q)$ is considered. Therefore, to the lowest order, $g_{\mathbf{k}_\perp}$ is independent of ζ so that we write $g_{\mathbf{k}_\perp} \simeq \overline{g}_{\mathbf{k}_\perp} \equiv h(x,\theta,\varepsilon,\mu)$. Here, the characteristic gradient scale length of h in the x-direction is on the order of the equilibrium gradient scale length and that x-dependence should be distinguished from the rapid variation described by the factor e^{ik_rx}. The equation for h is derived from Eq. (2) with the averaging operation in Eq. (7) as

$$\left(\frac{\partial}{\partial t} + \omega_\theta\frac{\partial}{\partial\theta} + ik_r\overline{v}_{dr}\right)h = F_0\overline{\left(J_0\frac{e}{T}\frac{\partial\phi_{\mathbf{k}_\perp}}{\partial t} + S_{\mathbf{k}_\perp}\right)}. \tag{12}$$

In the present work, we consider the case, in which the poloidal Mach number defined by $M_p \equiv |(cE_r/B_0r_0)(R_0q/v_t)|$ with $v_t \equiv (T/m)^{1/2}$ is much smaller than the unity. Then, for particles with $\kappa^2 > 1$, which are not trapped in helical ripples, the contribution of parallel motion to the poloidal angular velocity ω_θ is much larger than that of the $\mathbf{E}\times\mathbf{B}$ drift and the E_r term in Eq. (11) for $\kappa^2 > 1$ is neglected. Now, Eq.(12) is rewritten for $\kappa^2 > 1$ as

$$\left(\frac{\partial}{\partial t} + \omega_\theta\frac{\partial}{\partial\theta}\right)\left(e^{ik_r\Delta_r}h\right) = e^{ik_r\Delta_r}F_0\overline{\left(J_0\frac{e}{T}\frac{\partial\phi_{\mathbf{k}_\perp}}{\partial t} + S_{\mathbf{k}_\perp}\right)}, \tag{13}$$

where h is regarded as a function of θ, ε, μ, and $\sigma \equiv v_\parallel/|v_\parallel|$. In Eq. (13),

$$\Delta_r(\theta,\varepsilon,\mu) = \sigma\frac{qM}{2\pi}\frac{mc}{e\psi'}[J(\varepsilon,\theta,\mu) - J_t(\varepsilon,\mu)] \quad (\text{for } \kappa^2 > 1) \tag{14}$$

represents the radial displacement of the helical-ripple-averaged gyrocenter position and J_t is defined below. For $\kappa^2 > 1$, particles are classified into two types, particles trapped by the toroidicity and passing particles. Figure 2 (a) shows the (θ,κ^2)-plane, where regions for different classes of particles are divided by three boundary lines C_1, C_2, and C_3. In this figure, we consider the radial position $r = r_0$ (or $x = 0$) and assume that the profile of the magnetic-field strength along the field is similar to that of Fig. 1, where the maximum field strength B_M is given at $\theta = \pi$. The line C_1 is defined by $\kappa^2 = 1$ while C_2 is defined by Eq. (6) with $\varepsilon = \mu B_M \equiv \mu B_0[1-\epsilon_T(\pi)+\epsilon_H(\pi)]$ (recall that $x = 0$ is assumed). Passing particles are defined by $\varepsilon > \mu B_M$ and they belong to the region above C_2. On the other hand, toroidally-trapped particles are defined by $\varepsilon < \mu B_M$ with $\kappa^2 > 1$ and their region are bounded between C_1 and C_2. The trapping parameter κ^2 for $x = 0$ is written as $\kappa^2 = \kappa^2(\lambda,\theta) \equiv [1-\lambda B_0\{1-\epsilon_T(\theta)-\epsilon_H(\theta)\}]/[2\lambda B_0\epsilon_H(\theta)]$, where $\lambda = \mu/\varepsilon$. We note that κ^2 is an even function of θ. Toroidally-trapped particles, which have the two invariants ε and μ, reach the boundary line C_1 at the poloidal angles $\theta = \pm\theta_t(\lambda)$. The angle $\theta_t(\lambda)$ is determined by the condition $\kappa^2(\lambda,\theta_t(\lambda)) = 1$ and $\theta_t(\lambda) \geq 0$. Now, J_t in Eq. (14) is defined by $J_t(\varepsilon,\mu) = J(\theta_t(\mu/\varepsilon),\varepsilon,\mu)$ for toroidally trapped particles and by $J_t(\varepsilon,\mu) = J(\pi,\varepsilon,\mu)$ for passing particles.

For particles with $\kappa^2 < 1$, which are trapped in helical ripples, it is convenient to use J instead of ε as one of the phase-space coordinates for representing h. Again, considering the radial position $x = 0$, the energy variable ε is expressed as

$$\varepsilon = W(\theta,J,\mu) \equiv H(\theta,x=0,\mu,J) \equiv \mu B_0[1-\epsilon_T(\theta)+\epsilon_H\{2\kappa^2(\theta,J,\mu)-1\}], \tag{15}$$

where $\kappa^2(\theta,J,\mu)$ is implicitly defined from Eq. (8) for $\kappa^2 < 1$. As an approximate solution of Eq. (8) for κ^2 in the region $0 \leq \kappa^2 < 1$, we obtain

$$\kappa^2(\theta,J,\mu) \simeq C_\kappa X(\theta,J,\mu) - (C_\kappa - 1)[X(\theta,J,\mu)]^2, \tag{16}$$

where $X(\theta,J,\mu) \equiv J/[16(R_0/M)\{\mu B_0\epsilon_H(\theta)/m\}^{1/2}]$. The dimensionless numerical coefficient C_κ in Eq. (16) is given as $C_\kappa = 1.32984$ by using the least-mean-square method. Equation (16) is useful when we need an explicit form of $W(\theta,J,\mu)$ in Eq. (15). From Eqs. (10) and (11), we find

$$\left(\omega_\theta\frac{\partial}{\partial\theta} + ik_r\overline{v}_{dr}\right)h(\theta,J,\mu) = \left(\omega_\theta\frac{\partial}{\partial\theta} + ik_r\overline{v}_{dr} + eE_r\overline{v}_{dr}\frac{\partial}{\partial\varepsilon}\right)h(\theta,\varepsilon,\mu). \tag{17}$$

In the right-hand side of Eq. (17), the last term is regarded as negligibly small compared to the second term because of the order estimation $eE_r\partial/\partial\epsilon \sim e\Phi/(rT) \ll k_r$. Now, Eq. (12) is rewritten for $\kappa^2 < 1$ in the similar form to Eq. (13) as

$$\left(\frac{\partial}{\partial t} + \omega_\theta \frac{\partial}{\partial \theta}\right)\left(e^{ik_r\Delta_r} h_0(\theta, J, \mu)\right) = e^{ik_r\Delta_r} F_0 \overline{\left(J_0 \frac{e}{T}\frac{\partial \phi_{\mathbf{k}_\perp}}{\partial t} + S_{\mathbf{k}_\perp}\right)}, \tag{18}$$

where J is used as one of the independent variables instead of ε in Eq. (13) and the radial displacement of the bounce center of the helical-ripple-trapped particle is written as

$$\Delta_r(\theta, J, \mu) = \frac{1}{eE_r}[W(\theta, J, \mu) - W_t(J, \mu)] \quad (\text{for } \kappa^2 < 1) \tag{19}$$

where $W(\theta, J, \mu)$ is given by Eq. (15) and $W_t(J, \mu)$ is defined below. As shown in Fig. 2 (a), the particle region $\kappa^2 < 1$ is divided by the curve C_3 into two regions. Here, the equation to define C_3 is given by substituting $J = J_c(\mu) \equiv 16(R/M)(\mu B_0 \epsilon_{H0}/m)^{1/2}$ into the left-hand side of Eq. (8) for $\kappa^2 < 1$, where $\epsilon_{H0} = \epsilon_H(0)$ in the case of Fig. 2 (a). In the region below C_3 where $J < J_c(\mu)$, bounce centers of helical-ripple-trapped particles can make poloidally-closed orbits while, in the region between C_1 and C_3 where $\kappa^2 < 1$ and $J > J_c(\mu)$, bounce centers show poloidal drifts only in the bounded poloidal regions [$|\theta| > \theta_t$ in the case of Fig. 2 (a)]. In Fig. 2 (a), two points P_+ and P_- are located at the boundary poloidal angles $\theta = \theta_t$ and $-\theta_t$, respectively. Here, θ_t can be written as a function of (J, μ), $\theta_t = \theta_t(J, \mu)$, which is derived from the relation obtained by taking the limit $\kappa^2 \to 1$ in Eq. (8) for $\kappa^2 < 1$. Now, W_t in Eq. (19) is defined by $W_t(J.\mu) = W(\theta_t(J, \mu), J, \mu)$ for $J > J_c(\mu)$ and by $W_t(J, \mu) = W(0, J, \mu)$ for $J < J_c(\mu)$.

It is important to note that, on the boundary line $C_1(\kappa^2 = 1)$, particles can make transitions between toroidally-trapped and helical-ripple-trapped states. Figure 2 (b) shows poloidal cross sections of toroidally-trapped and helically-trapped orbits, between which transitions can occur. For the case of Figs. 2 (a) and (b), where $E_r > 0$ is assumed, both toroidally-trapped particles with $v_\parallel > 0$ and helical-ripple-trapped particles show the transition to toroidally-trapped particles with $v_\parallel < 0$ at the point P_+ where $\theta = \theta_t$. On the other hand, at the point P_- where $\theta = -\theta_t$, toroidally-trapped particles with $v_\parallel < 0$ change the sign of $v_\parallel$ or make the transition to helical-ripple-trapped particles. Although $E_r > 0$ is assumed throughout the present work, we can treat the case of $E_r < 0$ in the same manner as here by noting that the transition from the toroidally-trapped state with $v_\parallel > 0$ to the helically-trapped state occurs at P_+ for $E_r < 0$. Using the theory by Cary, *et al.* [14, 27], the probability P_t of the transition from toroidally-trapped ($v_\parallel < 0$) to helical-ripple-trapped particles at P_- is given by

$$P_t = \left[\frac{(\partial J_{r0}/\partial x)(\partial \varepsilon_x/\partial\theta) - (\partial J_{r0}/\partial\theta)(\partial\varepsilon_x/\partial x)}{(\partial J_{-0}/\partial x)(\partial\varepsilon_x/\partial\theta) - (\partial J_{-0}/\partial\theta)(\partial\varepsilon_x/\partial x)}\right]_{\theta=-\theta_t}, \tag{20}$$

where

$$J_{r0} \equiv \lim_{\kappa^2\to 1-0} J, \quad J_{-0} \equiv \lim_{\kappa^2\to 1+0} J(\sigma = -1), \quad \varepsilon_x \equiv \mu B_0[1 - \epsilon_T(\theta) + \epsilon_H(\theta)] - eE_r x. \tag{21}$$

We note that the fractional expression inside the brackets $[\cdots]$ in the right-hand side of Eq. (20) is an even function of θ so that it takes the same value at $\theta = \theta_t$ and $-\theta_t$. Now, using Eqs. (8), (20), and (21), we obtain

$$P_t \simeq \frac{4\sqrt{2}}{\pi} M_p \left(\frac{v}{v_t}\right)^{-1} \left[\epsilon_H^{-1/2} \frac{\partial \epsilon_H/\partial\theta}{\partial(\epsilon_H - \epsilon_T)/\partial\theta}\right]_{\theta=\theta_t}. \tag{22}$$

Here, we find that $P_t \ll 1$ because of the smallness of M_p. Even though $P_t \ll 1$, the average time duration which particles spend in the helically-trapped state is comparable to that in the toroidally-trapped state because the poloidal angular velocity ω_θ is slower in the former state than in the latter by a factor proportional to $M_p(\ll 1)$. For those particles [in the regions between C_2 and C_3 in Fig. 2 (a)] which make transitions, we define the average poloidal time period $\tau_{\rm po}$ by

$$\begin{aligned}\tau_{\rm po} &\equiv \sum_{\sigma=\pm 1}\left[H(-\sigma)\int_{|\theta|<\theta_t}\frac{d\theta}{|\omega_\theta|} + H(\sigma)(1-P_t)\int_{|\theta|<\theta_t}\frac{d\theta}{|\omega_\theta|}\right] + P_t\int_{|\theta|>\theta_t}\frac{d\theta}{|\omega_\theta|} \\ &\simeq \oint \frac{d\theta}{|\omega_\theta|}\left[2H(\kappa^2-1) + P_t\, H(1-\kappa^2)\right]\end{aligned} \tag{23}$$

and the poloidal-orbit average of an arbitrary function A defined along toroidally-trapped and helically-trapped orbits by

$$\begin{aligned}\langle A\rangle_{\rm po} &\equiv \frac{1}{\tau_{\rm po}}\sum_{\sigma=\pm 1}\left[H(-\sigma)\int_{|\theta|<\theta_t}\frac{A\, d\theta}{|\omega_\theta|} + H(\sigma)(1-P_t)\int_{|\theta|<\theta_t}\frac{A\, d\theta}{|\omega_\theta|}\right] + P_t\int_{|\theta|>\theta_t}\frac{A\, d\theta}{|\omega_\theta|} \\ &\simeq \frac{1}{\tau_{\rm po}}\oint\frac{d\theta}{|\omega_\theta|}\left[H(\kappa^2-1)\sum_{\sigma=\pm 1} A + H(1-\kappa^2)P_t A\right]\end{aligned} \tag{24}$$

where H is the Heaviside step function [$H(x) = 1$ for $x > 0$ and 0 for $x < 0$] and $\sigma \equiv v_\parallel/|v_\parallel|$. Also, recall that $\omega_\theta = -cE_r/(B_0 r_0)$ for $\kappa^2 < 1$ and $2\pi\sigma/(qM\tau_h)$ for

$\kappa^2 > 1$. When the transition occurs between at $C_1(\kappa^2 = 1)$, the independent variable J for A in the helical-ripple-trapped state and the independent variable ε for A in the toroidally-trapped state are connected to each other by the relation that is defined by substituting $\theta = \theta_t(\lambda)$ and $\lambda = \mu/\varepsilon$ into Eq. (15) as

$$\varepsilon = W(\theta_t(\mu/\varepsilon), J, \mu). \tag{25}$$

By the operation defined in Eq. (24), the function A is averaged over the connected orbits containing both parts of toroidally-trapped and helical-ripple-trapped states so that $\langle A\rangle_{\rm po}$ is independent of θ and it is regarded as a function of either (ε, μ) or (J, μ), where ε and J are related to each other by Eq. (25).

For passing particles [in the region above C_2 in Fig. 2 (a)] and helical-ripple-trapped particles which make poloidally-closed orbits (below C_3), $\tau_{\rm po}$ and $\langle A\rangle_{\rm po}$ are given by

$$\tau_{\rm po} \equiv \oint \frac{d\theta}{|\omega_\theta|} \quad \text{and} \quad \langle A\rangle_{\rm po} \equiv \frac{1}{\tau_{\rm po}} \oint \frac{A\, d\theta}{|\omega_\theta|}, \tag{26}$$

respectively.

The present work is concerned with the long-time behavior of zonal flows and the characteristic time scale is assumed to be much longer than $1/\omega_\theta$. To the lowest order, Eqs. (13) and (18) are both written in the same form as $\omega_\theta \partial \left(e^{ik_r\Delta_r} h\right)/\partial\theta = 0$, which implies $e^{ik_r\Delta_r} h$ is independent of θ. Here, we should recall that ε is used as the independent variable of h for $\kappa^2 > 1$ while J is for $\kappa^2 < 1$. Then, using the poloidal-orbit average [defined in Eqs. (24) and (26)], integrating Eqs. (13) and (18) in time, and using Eq. (4) with $g_{\mathbf{k}_\perp} \simeq \overline{g}_{\mathbf{k}_\perp} \equiv h$, we obtain

$$\begin{aligned}
&\left\langle e^{ik_r\Delta_r} h(t)\right\rangle_{\rm po} \\
&= \left\langle e^{ik_r\Delta_r}[h(0) + F_0\overline{R_{\mathbf{k}_\perp}(t)}]\right\rangle_{\rm po} \\
&\quad + \frac{e}{T}F_0\left\langle e^{ik_r\Delta_r}\overline{J_0\left\{\phi_{\mathbf{k}_\perp}(t) - \phi_{\mathbf{k}_\perp}(0)\right\}}\right\rangle_{\rm po} \\
&= \left\langle e^{ik_r\Delta_r}\overline{[\delta f^{\rm (g)}_{\mathbf{k}_\perp}(0) + F_0 R_{\mathbf{k}_\perp}(t)]}\right\rangle_{\rm po} \\
&\quad + \frac{e}{T}F_0\left\langle e^{ik_r\Delta_r}\overline{J_0\phi_{\mathbf{k}_\perp}(t)}\right\rangle_{\rm po},
\end{aligned} \tag{27}$$

where $R_{\mathbf{k}_\perp}(t) \equiv \int_0^t S_{\mathbf{k}_\perp}(t')dt'$. Appendix A shows in detail how Eq. (27) is derived. Equation (27) is valid for all passing, toroidally-trapped, and helical-ripple-trapped states although we should regard Δ_r and $\langle\cdots\rangle_{\rm po}$ in Eq. (27) as functions of (ε, μ) for $\kappa^2 > 1$ and of (J, μ) for $\kappa^2 < 1$. In the regions between C_1 and C_3 in Fig. 2 (a), where the transitions occur at $C_1(\kappa^2 = 1)$, ε and J are related to each other by Eq. (25). Now, using Eqs. (3) and (27), the perturbed *particle* distribution function is written in the same form for all classes of particles as

$$\begin{aligned}
\delta f_{\mathbf{k}_\perp}(t) &= -\frac{e}{T}\phi_{\mathbf{k}_\perp}(t)F_0\left[1 - e^{-i\mathbf{k}_\perp\cdot\boldsymbol{\rho}}e^{ik_r\Delta_r}\left\langle e^{ik_r\Delta_r}\overline{J_0}\right\rangle_{\rm po}\right] \\
&\quad + e^{-i\mathbf{k}_\perp\cdot\boldsymbol{\rho}}e^{-ik_r\Delta_r}\left\langle e^{ik_r\Delta_r}\overline{[\delta f^{\rm (g)}_{\mathbf{k}_\perp}(0) + F_0 R_{\mathbf{k}_\perp}(t)]}\right\rangle_{\rm po},
\end{aligned} \tag{28}$$

where $\phi_{\mathbf{k}_\perp} = \langle\phi_{\mathbf{k}_\perp}\rangle$ is used. In the right-hand side of Eq. (28), the first group of terms proportional to $\phi_{\mathbf{k}_\perp}(t)$ represent the classical and neoclassical polarizations due to gyromotion and drift motion of particles while the second group of terms contain the initial condition and the turbulent source.

IV. COLLISIONLESS LONG-TIME ZONAL-FLOW RESPONSE IN THE PRESENCE OF THE EQUILIBRIUM ELECTRIC FIELD

In order to determine the zonal-flow potential, we use Poisson's equation written as

$$\int d^3v\ \delta f_{i\mathbf{k}_\perp} - \int d^3v\ \delta f_{e\mathbf{k}_\perp} = n_0\frac{e\phi_{\mathbf{k}_\perp}}{T_e}(k_\perp\lambda_{De})^2, \tag{29}$$

where the subscripts representing ions (i) and electrons (e) are explicitly shown and $\lambda_{De} \equiv [T_e/(4\pi n_0 e^2)]^{1/2}$ is the electron Debye length. Then, substituting Eq. (28) into (29) and taking its flux-surface average, we obtain

$$\frac{e\phi_{\mathbf{k}_\perp}(t)}{T_i} = \frac{\langle I(t)\rangle}{\mathcal{D}}, \tag{30}$$

which describes the collisionless long-time behavior of the zonal-flow potential. Here, $\langle\cdots\rangle$ denotes the flux-surface average and the shielding effects are represented by

$$\begin{aligned}
\mathcal{D} &= \sum_{a=i,e}\frac{T_i}{T_a}\left\langle\int d^3v\ F_{a0}\left[1 - \left|\left\langle e^{ik_r\Delta_{ar}}\overline{J_0(k_\perp\rho_a)}\right\rangle_{\rm po}\right|^2\right]\right\rangle \\
&\quad + n_0(T_i/T_e)(k_\perp\lambda_{De})^2,
\end{aligned} \tag{31}$$

while the initial conditions and the nonlinear sources are included in

$$\begin{aligned}
\langle I(t)\rangle &= \sum_{a=i,e}\frac{e_a}{e}\left\langle\int d^3v\ J_0(k_\perp\rho_a)e^{-ik_r\Delta_{ar}}\right. \\
&\quad \left.\times\left\langle e^{ik_r\Delta_{ar}}\overline{[\delta f^{\rm (g)}_{a\mathbf{k}_\perp}(0) + F_{a0}R_{a\mathbf{k}_\perp}(t)]}\right\rangle_{\rm po}\right\rangle.
\end{aligned} \tag{32}$$

It should be noted that Eqs. (30)–(32) can be applied to the zonal-flow potential in wide wave-number ranges including both ion temperature gradient (ITG) and electron temperature gradient (ETG) turbulence.

We now consider the wave-number region relevant to the ITG turbulence, where $k_\perp\rho_i < 1$, and take the small-electron-gyroradius limit $k_\perp\rho_e \to 0$. In this case, we also

have $k_\perp \lambda_{De} \to 0$ and Eq. (29) reduces to the quasineutrality condition. Here, we also assume the radial displacement of ions to be so small that $k_r \Delta_{ir} < 1$. Then, we put $k_r \Delta_{er} \to 0$ for $\kappa^2 > 1$, where $\Delta_{er} \ll \Delta_{ir}$ because of the small electron gyroradius, although electrons and ions in the helical-ripple-trapped states $\kappa^2 < 1$, for which $\overline{v}_{dre} \sim \overline{v}_{dri}$, make radial displacements of the same order of magnitude, $\Delta_{er} \sim \Delta_{ir}$. Then, Eqs. (31) and (32) are expanded in terms of $k_\perp \rho_i$ and $k_r \Delta_{ir}$ to yield

$$\begin{aligned}\mathcal{D} &= n_0 \left\langle k_\perp^2 \rho_{ti}^2 \right\rangle \\ &\quad + \sum_{a=i,e} \frac{T_i}{T_a} \left\langle \int d^3v \, F_{a0} k_r^2 \left\{ \langle \Delta_{ar}^2 \rangle_{\rm po} - \langle \Delta_{ar} \rangle_{\rm po}^2 \right\} \right\rangle \\ &= n_0 \left\langle k_\perp^2 \rho_{ti}^2 \right\rangle \left[1 + G_p + G_t + M_p^{-2} (G_{ht} + G_h)(1 + T_e/T_i) \right] \end{aligned} \tag{33}$$

and

$$\begin{aligned}\langle I(t) \rangle &= \left\langle \int d^3v \, \left[1 + i k_r \left\{ \Delta_{ir} - \langle \Delta_{ir} \rangle_{\rm po} \right\} \right] \right. \\ &\quad \left. \times \overline{[\delta f_{i\mathbf{k}_\perp}^{(\rm g)}(0) + F_{i0} R_{i\mathbf{k}_\perp}(t)]} \right\rangle , \end{aligned} \tag{34}$$

respectively, where $\rho_{ti} \equiv (T_i/m_i)^{1/2}/\Omega_i$ denotes the ion thermal gyroradius and the electron contribution to $\langle I(t) \rangle$ is neglected. The part proportional to T_e/T_i in Eq. (33) represents contributions from electrons trapped in helical ripples. The dimensionless geometrical factors G_p, G_t, G_{ht}, and G_h in Eq. (33) are defined by

$$\begin{aligned} G_p &= \frac{12}{\pi^3} B_0 R_0^2 q^2 \left\langle \frac{B^2}{|\nabla \psi|^2} \right\rangle \left[\int_0^{1/B_M} d\lambda \right. \\ &\quad \times \oint \frac{d\theta}{2\pi} (2\lambda B_0 \epsilon_H)^{-1/2} \kappa^{-1} K(\kappa^{-1}) \left\{ (2\lambda B_0 \epsilon_H)^{1/2} \right. \\ &\quad \left. \left. \times \kappa E(\kappa^{-1}) - \frac{\oint \frac{d\theta}{2\pi} K(\kappa^{-1}) E(\kappa^{-1})}{\oint \frac{d\theta}{2\pi} (2\lambda B_0 \epsilon_H)^{-1/2} \kappa^{-1} K(\kappa^{-1})} \right\}^2 , \\ G_t &= \frac{3}{\pi^3} B_0 \left(\frac{R_0 q}{r_0} \right)^2 \int_{1/B_M}^{1/B'_m} \hat{\tau}_{\rm po}(\lambda) d\lambda \, \langle H(\kappa^2 - 1) \\ &\quad \times [\{\epsilon_H(\theta)\}^{1/2} \kappa E(\kappa^{-1}) - \{\epsilon_H(\theta_t(\lambda))\}^{1/2}]^2 \rangle_{\rm po}, \\ G_{ht} &= \frac{15}{32\pi} B_0 \left(\frac{R_0 q}{r_0} \right)^2 \int_{1/B_M}^{1/B'_m} \hat{\tau}_{\rm po}(\lambda) d\lambda \, \langle H(1 - \kappa^2) \\ &\quad \times \{\epsilon_*(\theta, \lambda)\}^2 \rangle_{\rm po} - \langle H(1 - \kappa^2) \epsilon_*(\theta, \lambda) \rangle_{\rm po}^2], \\ G_h &= \frac{15}{\sqrt{2}\,\pi} \left(\frac{R_0 q}{r_0} \right)^2 (\epsilon_{H0})^{1/2} \left[\langle (\widetilde{\epsilon_T} + \widetilde{\epsilon_H})^2 \rangle_{\rm po} \right. \\ &\quad - 2 C_\kappa (\epsilon_{H0})^{1/2} \langle \widetilde{(\epsilon_H)^{1/2}} (\widetilde{\epsilon_T} + \widetilde{\epsilon_H}) \rangle_{\rm po} \\ &\quad \left. + \frac{4}{3} C_\kappa^2 \epsilon_{H0} \langle \{ \widetilde{(\epsilon_H)^{1/2}} \}^2 \rangle_{\rm po} \right] , \end{aligned} \tag{35}$$

where B_M denotes the maximum field strength over the flux surface and B'_m represents the minimum value of local maximum field strengths within each helical ripple. For the case of Fig. 1, $B_M = B_0[1 - \epsilon_T(\pi) + \epsilon_H(\pi)]$ and $B'_m = B_0[1 - \epsilon_T(0) + \epsilon_H(0)]$. Here, G_p and G_t are related to passing and toroidally-trapped particle orbits, respectively, while G_h and G_{ht} originate from poloidally-closed and unclosed orbits of helical-ripple-trapped particles, respectively. Integrals of functions of λ and θ are required to calculate these geometrical factors in Eq. (35), where $\hat{\tau}_{\rm po}(\lambda)$ and $\epsilon_*(\theta, \lambda)$ is defined by

$$\begin{aligned} &\hat{\tau}_{\rm po}(\lambda) \equiv \frac{v \tau_{\rm po}}{R_0 q} \\ &\equiv 4\sqrt{2} \oint \frac{d\theta}{2\pi} \left(H(\kappa^2 - 1) \{\epsilon_H(\theta)\}^{-1/2} \kappa^{-1} K(\kappa^{-1}) \right. \\ &\quad \left. + 2 \, H(1 - \kappa^2) \left[\epsilon_H^{-1/2} \frac{\partial \epsilon_H / \partial \theta}{\partial (\epsilon_H - \epsilon_T)/\partial \theta} \right]_{\theta = \theta_t} \right) , \end{aligned} \tag{36}$$

and

$$\begin{aligned} \epsilon_*(\theta, \lambda) &= \epsilon_T(\theta) + \epsilon_H(\theta) - 2 C_\kappa \{\epsilon_T(\theta) \epsilon_H(\theta_t(\lambda))\}^{1/2} \\ &\quad + (2C_\kappa - 1) \epsilon_H(\theta_t(\lambda)) - \epsilon_T(\theta_t(\lambda)), \end{aligned} \tag{37}$$

respectively. The poloidal-angle functions $\widetilde{\epsilon_T}$, $\widetilde{\epsilon_H}$, and $\widetilde{(\epsilon_H)^{1/2}}$, which are used to define G_h, are given by

$$\begin{aligned} &\widetilde{\epsilon_T} = \epsilon_T - \langle \epsilon_T \rangle_{\rm po}, \quad \widetilde{\epsilon_H} = \epsilon_H - \langle \epsilon_H \rangle_{\rm po} \\ &\widetilde{(\epsilon_H)^{1/2}} = (\epsilon_H)^{1/2} - \langle (\epsilon_H)^{1/2} \rangle_{\rm po}. \end{aligned} \tag{38}$$

The radial displacements Δ_r of helical-ripple-trapped particles, which give main contributions to the shield of the zonal-flow potential, are proportional to the radial drift velocities $\overline{v}_{dr}$ of those particles but inversely proportional to the radial electric field E_r. In helical configurations optimized for reducing neoclassical transport, helical-ripple-trapped particles have small v_{dr} so that G_{ht} and G_h take small values and the zonal-flow potential shows a good response to the turbulent source. Effects of E_r on Δ_r and accordingly on the zonal-flow response are shown by the poloidal Mach number $M_p \equiv |(cE_r/B_0 r_0)(R_0 q/v_{ti})|$ in Eq. (33). As seen from Eq. (33), the shield of the zonal-flow potential is weakened by strengthening the radial electric field E_r and accordingly increasing M_p. For the same value of E_r, M_p can also be increased also by using ions with a heavier mass, which is expected to produce zonal flows more efficiently and give a more favorable ion-mass dependence of the ITG turbulent transport than the conventional gyro-Bohm scaling. In order to physically understand the above-mentioned ion-mass dependence of the zonal-flow response, we should note that the geometrical factors multiplied with M_p^{-2} represent the ratio of the neoclassical polarization $\propto (\epsilon_H)^{1/2} (k_r \Delta_r)^2$ due to radial drift of helical-ripple-trapped particles to the classical polarization $\propto (k_r \rho_i)^2$. This ratio becomes smaller for heavier ions because the classical polarization is proportional to the ion mass while the neoclassical polarization is independent of the mass in the presence of the equilibrium radial electric field.

If we assume the initial perturbed ion gyrocenter distribution function to take the Maxwellian form $\delta f^{(g)}_{i\mathbf{k}_\perp}(0) = (\delta n^{(g)}_{i\mathbf{k}_\perp}(0)/n_0)F_{i0}$ with $\delta n^{(g)}_{i\mathbf{k}_\perp}(0) = n_0(k_\perp^2\rho_{ti}^2)(e\phi_{\mathbf{k}_\perp}(0)/T_i)$ given by the quasineutrality condition, the relation of the residual zonal-flow potential at time t to its initial value is derived from Eqs. (30), (33), and (34) as

$$\phi(t) = \frac{\phi(0)}{1 + G_p + G_t + M_p^{-2}(G_{ht} + G_h)(1 + T_e/T_i)}, \tag{39}$$

where contributions of the nonlinear source are dropped. In our previous works [7, 8] about the zonal-flow response in helical systems without E_r, the potential shielding by helical-ripple-trapped particles has a different dependence on $k_r\rho_{ti}$ and the residual zonal-flow potential normalized by the initial value, $\phi(t)/\phi(0)$, decreases with decreasing $k_r\rho_{ti}$. Now, Eq. (39) shows that, in the presence of the poloidal $\mathbf{E}\times\mathbf{B}$ rotation of helical-ripple-trapped particles, $\phi(t)/\phi(0)$ becomes independent of $k_r\rho_{ti}$ for $k_r\rho_{ti} \ll 1$, which is a similar result to the residual zonal-flow potential obtained by Rosenbluth and Hinton for the tokamak case [3].

In the single-helicity helical configuration, where ϵ_H is independent of θ, the curve C_3 coincides with C_1 in Fig. 2 (a) and all helical-ripple-trapped particles show poloidally-closed orbits. Then, we have $G_{ht} = 0$ and Eq. (40) reduces to

$$\phi(t) = \frac{\phi(0)}{1 + G_{pt} + (15/4\pi)M_p^{-2}q^2(2\epsilon_H)^{1/2}(1 + T_e/T_i)}, \tag{40}$$

where $\epsilon_T = (r_0/R_0)\cos\theta$ is used. Equation (40) corresponds to the one derived in our previous work [note that a numerical coefficient $15/8\pi$ in Eq.(12) of [18] is corrected as $15/4\pi$ here]. In this case, $G_{pt} \equiv G_p + G_t$ becomes the same geometrical factor as given by Eq. (52) in Ref. [8]. Also, Eq. (40) agrees with the theory by Mynick and Boozer [10] in which transitions of particles between different classes of orbits are not taken into account.

In the limit $E_r \to 0$ as in our previous works [7, 8], we have $|k_r\Delta_r| \to \infty$ for helical-ripple-trapped particles and the nonadiabatic part of the helically-trapped-particle distribution function is strongly damped by the phase mixing due to the bounce-center radial drift. Then, the terms of the form $\langle e^{ik_r\Delta_r}\cdots\rangle_{\rm po}$ in Eqs. (27), (28), (31), and (32) vanish in helically-trapped regions and the previous results in Refs. [7, 8] can be reproduced from Eq. (30)–(32).

The results shown in Eqs. (33), (39) and (40) do not change when the sign of E_r is changed. It is because contributions of the magnetic ∇B-curvature drift velocity to the poloidal rotation are neglected compared to the $\mathbf{E}\times\mathbf{B}$ rotation. When the poloidal rotation due to the magnetic drift is added to the $\mathbf{E}\times\mathbf{B}$ rotation, the total poloidal rotation is either strengthened or weakened depending on the particle charge and on which class the particle orbit belongs to. For example, in the case of $E_r > 0$ and helical-rippled-trapped particles with unclosed orbits [see Fig. 2 (b)], the poloidal rotation driven by the $\mathbf{E}\times\mathbf{B}$ drift is weakened by the magnetic drift for ions but strengthened for electrons although the relation between the $\mathbf{E}\times\mathbf{B}$ and magnetic poloidal drifts is reversed by changing the sign of E_r. The variation of the particle rotation speed will change the particle radial displacement and accordingly the shielding of the zonal-flow potential. Effects of the poloidal magnetic drift on the zonal-flow response are neglected as a small correction in the present work although they can be included in direct numerical simulations which may show a subtle dependence of the residual zonal flow on the sign of E_r.

V. CONCLUSIONS

In the present paper, collisionless long-time behaviors of zonal flows in helical systems with radial electric fields are theoretically investigated. All classes of particles in passing, toroidally-trapped, and helical-ripple-trapped states are taken into account to derive the long-time response of the zonal-flow potential to the initial condition and to the turbulence source. Helical-ripple-trapped particles can draw either poloidally-closed or unclosed orbits, to the latter of which toroidally-trapped particles can make transition with some probability. Effects of this transition probability are also included in our theory. Resultant formulas in Eqs. (30)–(35) describe how the long-time zonal-flow response depends on the helical geometry and on the equilibrium radial electric field E_r. The dependence on E_r appears through the poloidal Mach number $M_p \equiv |(cE_r/B_0r_0)(R_0q/v_t)|$. By doing neoclassical optimization of the helical geometry to lower the radial drift or by strengthening the radial electric field E_r to boost the poloidal rotation, we can reduce the radial displacements of helical-ripple-trapped particles and accordingly enhance the zonal-flow response. Furthermore, under the same conditions on the geometry and the magnitude of E_r, using ions with a heavier mass increases M_p and leads to a higher zonal-flow response so that we can expect a more favorable ion-mass dependence of the turbulent transport than the conventional gyro-Bohm scaling.

For gyrokinetic simulation to examine effects of the $\mathbf{E}\times\mathbf{B}$ drift of helical-ripple-trapped particles, a simulation domain needs to be extended from a toroidal flux-tube to a poloidally-global region. In order to confirm the validity of our theoretical predictions presented in this work, simulation studies using the poloidally-global gyrokinetic Vlasov code [19] are now in progress and their results will be reported elsewhere.

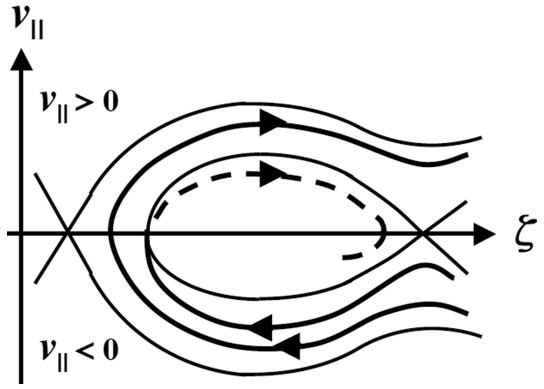

FIG. 3: The $(\zeta, v_\parallel)$ phase space obtained by magnifying the neighborhood of the transition point P_-. Two toroidally-trapped orbits (solid curves with arrows) are shown in the $v_\parallel < 0$ region. One of them is connected to a toroidally-trapped orbit in the $v_\parallel > 0$ region while the other is coupled to a helically-trapped orbit (a dashed curve with an arrow). The latter case represents the transition from the toroidally-trapped state to the helically-trapped state.

Acknowledgments

The authors thank Dr. M. Yokoyama for useful discussions on particle orbits in helical systems. This work is supported in part by the Japanese Ministry of Education, Culture, Sports, Science, and Technology, Grant No. 17360445 and in part by the NIFS Collaborative Research Programs, NIFS08KDAD008, NIFS08KNXN145, and NIFS08KTAL006.

APPENDIX A: DERIVATION OF EQ. (27)

For passing particles and helically-trapped particles with closed orbits, Eq. (27) is immediately derived from Eq. (13) and from Eq. (18), respectively, with using the orbit-average defined in Eq. (26) and the time integration. Therefore, it is shown in this Appendix how to derive Eq. (27) only for particles which show transitions between toroidally-trapped and helically-trapped states. We should recall that Eqs. (13) and (18) are both derived by taking an average within a helical ripple [see Eq. (7)] and, therefore, $h = \overline{g}_{\mathbf{k}_\perp}$ is independent of ζ. Figure 3 shows the $(\zeta, v_\parallel)$ phase space obtained by magnifying the neighborhood of the transition point P_- [see Figs. 2 (a) and (b)]. There, two toroidally-trapped orbits (solid curves with arrows) are seen in the $v_\parallel < 0$ region. One of them is connected to a toroidally-trapped orbit in the $v_\parallel > 0$ region while the other is coupled to a helically-trapped orbit (a dashed curve). The latter case represents the transition from the toroidally-trapped state to the helically-trapped state. These two types of particle orbits should be taken into account when we evaluate $h = \overline{g}_{\mathbf{k}_\perp}$ in the neighborhood of transition point. For toroidally-trapped particles, which don't show transitions to the helically-trapped state but change the sign of $v_\parallel$, the boundary condition at P_- is given by

$$(g_{\mathbf{k}_\perp})_{t-} = (g_{\mathbf{k}_\perp})_{t+}, \tag{A1}$$

where the subscripts $t-$ and $t+$ represent toroidally-trapped particles with $v_\parallel < 0$ and those with $v_\parallel > 0$, respectively. On the other hand, for particles which show transitions between the toroidally-trapped and helically-trapped states, we have

$$(g_{\mathbf{k}_\perp})_{t-} = (g_{\mathbf{k}_\perp})_{r}, \tag{A2}$$

where the subscript r represents the helical-ripple-trapped state. Recalling that the probability of the transition from the toroidally-trapped state to the helically-trapped state is given by P_t in Eq. (22), $h = \overline{g}_{\mathbf{k}_\perp}$ is considered to satisfy the boundary condition written as

$$h_{t-} = (1 - P_t)\, h_{t+} + P_t\, h_r. \tag{A3}$$

The boundary condition in Eq. (A3) at the transition point P_- can also be used at P_+ [see Figs. 2 (a) and (b)] as seen by making a similar argument for the transition at P_+. Now, applying the average operation in Eq. (24) to a combined set of Eqs. (13) and (18) and noting from Eqs. (14) and (19) that $\Delta_r = 0$ at P_+ and P_-, we find from Eq. (A3) that the term $\langle \omega_\theta \partial (e^{ik_r\Delta_r} h)/\partial\theta \rangle_{\rm po}$ vanishes and

$$\frac{\partial}{\partial t} \left\langle e^{ik_r\Delta_r} h \right\rangle_{\rm po} = \left\langle e^{ik_r\Delta_r} F_0 \overline{\left(J_0 \frac{e}{T} \frac{\partial \phi_{\mathbf{k}_\perp}}{\partial t} + S_{\mathbf{k}_\perp} \right)} \right\rangle_{\rm po}. \tag{A4}$$

Integrating Eq. (A4) in time immediately yields Eq. (27).

[1] P. H. Diamond, S.-I. Itoh, K. Itoh, and T. S. Hahm, Plasma Phys. Control. Fusion **47**, R35 (2005).
[2] K. Itoh, S.-I. Itoh, P. H. Diamond, A. Fujisawa, G. R. Tynan, M. Yagi, and Y. Nagashima, Phys. Plasmas **13**, 055502 (2006).
[3] M. N. Rosenbluth and F. L. Hinton, Phys. Rev. Lett. **80**, 724 (1998).
[4] Y. Xiao and P. J. Catto, Phys. Plasmas **13**, 082307 (2006).
[5] P. Angelino, X. Garbet, L. Villard, A. Bottino, S. Jolliet, Ph. Ghendrih, V. Grandgirard, B. F. McMillan, Y. Sarazin, G. Dif-Pradalier, and T. M. Tran, Phys. Plasmas **15**, 062306 (2008).
[6] Z. Gao, P. Wang, and H. Sanuki, Phys. Plasmas **15**, 074502 (2008).
[7] H. Sugama and T.-H. Watanabe, Phys. Rev. Lett. **94**,

115001 (2005).
[8] H. Sugama and T.-H. Watanabe, Phys. Plasmas **13**, 012501 (2006).
[9] S. Ferrando-Margalet, H. Sugama and T.-H. Watanabe, Phys. Plasmas **14**, 122505 (2007).
[10] H. E. Mynick and A. H. Boozer, Phys. Plasmas **14**, 072507 (2007).
[11] A. Mishchenko, P. Helander, and A. Könies, Phys. Plasmas **15**, 072309 (2008).
[12] T. Watari, Y. Hamada, T. Notake, N. Takeuchi, and K. Itoh, Phys. Plasmas **13**, 062504 (2006).
[13] K. C. Shaing and S. A. Hokin, Phys. Fluids **26**, 2136 (1983).
[14] M. Wakatani, *Stellarator and Heliotron Devices* (Oxford University Press, Oxford, 1998), Chaps. 6 and 7.
[15] H. Sugama and S. Nishimura, Phys. Plasmas **9**, 4637 (2002); H. Sugama and T.-H. Watanabe, *ibid.* **15**, 042502 (2008).
[16] T.-H. Watanabe, H. Sugama, and S. Ferrando-Margalet, Nucl. Fusion **47**, 1383 (2007).
[17] T.-H. Watanabe, H. Sugama, and S. Ferrando-Margalet, Phys. Rev. Lett. **100**, 195002 (2008).
[18] H. Sugama, T.-H. Watanabe, and S. Ferrando-Margalet, Plasma Fusion Res. **3**, 041 (2008).
[19] T.-H. Watanabe, H. Sugama, and S. Ferrando-Margalet, 22nd IAEA Fusion Energy Conference 2008, Geneva, Switzerland (IAEA, Vienna, 2008) TH/P8-20.
[20] O. Motojima, N. Ohyabu, A. Komori, *et al.*, Nucl. Fusion **43**, 1674 (2003).
[21] H. Yamada, A. Komori, N. Ohyabu, *et al.*, Plasma Phys. Control. Fusion **43**, A55 (2001).
[22] M. Yokoyama, J. Plasma Fusion Res. **78**, 205 (2002).
[23] H. E. Mynick, Phys. Plasmas **13**, 058102 (2006).
[24] D. A. Spong, S. P. Hirshman, L. A. Berry, *et al.*, Nucl. Fusion **41**, 711 (2001).
[25] J. N. Talmadge, V. Sakaguchi, F. S. B. Anderson, *et al.*, Phys. Plasmas **9**, 5165 (2001).
[26] G. Grieger, W. Lotz, P. Merkel, *et al.*, Phys. Fluids B **4**, 2081 (1992).
[27] J. R. Cary, C. L. Hedrick, and J. S. Tolliver, Phys. Fluids **31**, 1586 (1988).
[28] W. Horton, Rev. Mod. Phys. **71**, 735 (1999).
[29] E. A. Frieman and L. Chen, Phys. Fluids **25**, 502 (1982).
[30] R. D. Hazeltine and J. D. Meiss, *Plasma Confinement* (Addison-Wesley, Redwood City, California, 1992), p. 298.